Journal of Computer Engineering
ISSN 10003428

Original Research Article
Vol 11, Issue 7, 2022 | ISSN: 1000-3428

Development of an Analog Module for Hybrid Massive MIMO Testbeds Utilizing Beam Alignment Algorithms

Elena Vasquez and Liam R. McFadden

Elena Vasquez, Department of Electrical and Computer Engineering, University of Illinois at Urbana-Champaign, USA; Liam R. McFadden, School of Engineering, University of Bristol, United Kingdom

Abstract—Hybrid analog-digital beamforming for massive MIMO is an important technology for millimeter-wave communication systems. Current experimentation of massive MIMO is based mainly on full digital solutions and in the sub-6GHz frequency range. The technology for millimeter-wave massive MIMO systems is not yet available to the broad research community. Due to high path loss, sparsity of the channel, and restrictions of the hardware in the millimeter-wave band, new challenges in signal processing arise. One of these problems is the initial link acquisition also called beam alignment (BA). We present a hybrid analog-digital massive MIMO sub-6GHz testbed with 64 antennas. This testbed enables the investigation of challenges connected to a hybrid analog-digital architecture like the BA problem. We demonstrate multiple BA algorithms to show their advantages and disadvantages. The testbed is based on a self-developed analog module with a high resolution of phase and amplitude settings. Our module can be connected to standard software defined radios (SDRs) and supports different types of hybrid architectures.

I. Introduction and Motivation

Two of the main topics of the recent research for the next generation of mobile networks are multi-user massive MIMO and millimeter-wave communication [1]. An important challenge in millimeter-wave systems is the significant path loss compared to the current frequency bands of mobile networks (sub-6GHz) [2]. To compensate for the high path loss many antennas can be used to generate beamforming gain. Therefore massive MIMO is a targeted technology also for millimeter-wave systems. In comparison to sub-6GHz systems full digital massive MIMO millimeter-wave implementations with a large number of RF chains are currently power and cost restricted. Hybrid analog-digital beamforming is considered as a solution to this problem [3]. However, the recent advances in prototyping and experimentation for massive MIMO have mainly concentrated on full digital solutions and on frequency bands of current mobile networks (e.g. [4] and [5]). The technology for millimeter-wave radios with many antennas is currently investigated [6] but not yet accessible to the wide communication and signal processing research

community. To bridge the gap until millimeter-wave hybrid systems become feasible for signal processing research, we developed an analog beamforming module in the sub-6GHz frequency range. The module is compatible with state of the art software defined radios (SDRs) used in research (e.g., see [7]). It enables the investigation of problems arising with the use of a hybrid massive MIMO architecture. The results of such experimentation hopefully will accelerate the development and deployment of millimeter-wave systems.

One specific problem due to the high path loss and the sparsity in the angular domain of a millimeter-wave channel is the initial acquisition of the link between a base station (BS) and the user equipment (UE) [2]. This is more challenging than in the sub-6GHz case since beamforming at both sides is needed in order to provide a sufficient signal-to-noise ratio (SNR). Hence, both the BS and the UE must train their beams to point at an angle of arrival (AoA)/angle of departure (AoD) corresponding to a multipath component that conveys enough signal energy. On the other hand, the beam training must work at very low pre-beamforming SNR. We refer to the initial acquisition in millimeter-wave systems as beam alignment (BA). The demonstration will showcase multiple BA algorithms to show the capabilities of the analog module and to compare the performance of the algorithms in a real system.

II. System Description

The testbed implements a hybrid analog-digital massive MIMO system as for example described in [8]. Such a system can be used for multi user MIMO (MU-MIMO) or for a single user respectively point to point configuration. In this paper, we concentrate on the BS part of the communication system. The BS utilizes N_{BS} antennas and N_{RF} RF chains converting the analog RF signal to digital baseband streams. The demonstration at the conference showed the testbed with $N_{BS} = 64$ antennas and $N_{RF} = 2$ RF chains. The results shown in Section IV-B are taken with 32 antennas (2 rows, 16 columns) and 2 RF chains. The lower number of antennas was chosen to reduce the

How to cite: Elena Vasquez and Liam R. McFadden (2022). Development of an Analog Module for Hybrid Massive MIMO Testbeds Utilizing Beam Alignment Algorithms. Journal of Computer Engineering, 11(7), 67–79. DOI: https://doi.org/10.5281/zenodo.19345500

influence of near field effects on the measurements in the finite space of the indoor measurement location. The Fraunhofer distance for this antenna configuration and the used carrier frequency of 2.4GHz is 16m.

The testbed consists of 4 parts, the antenna, an analog beamforming part, the RF chains in the form of a SDR, and a host PC for control and digital signal processing. Figure 1 shows the testbed conceptually and Figure 2 is a picture during the measurement of the results of Section IV-B.

The antenna is an array of microstrip patches with a tunable center frequency between 2.2GHz and 2.5GHz. The antenna is build of panels of 2 by 8 elements with a spacing of $\lambda/2$ (at a frequency of 2.4GHz). Multiple panels can be arranged to form different antenna configurations like 2 by 16 or 4 by 8 elements.

The analog processing part of our testbed is divided into multiple analog modules (AMs). Such a modularization allows for scalability of the system, different array arrangements, and ease of development of the AM. An AM is a fully connected analog RF network between $N_{RF}^{AM} = 2$ ports connected to RF chains and $N_{BS}^{AM} = 16$ ports connected to antennas. A junction in this network is realized with a power divider respectively combiner. A fully connected network connects every RF chain port to every antenna port. Each path of this network has a variable phase and amplitude. The AM is introduced in Section III. To implement N_{BS} antennas and N_{RF} RF chains a system requires $N_{AM} = N_{RF}/N_{RFAM} \cdot N_{BS}/N_{BSAM}$ analog modules. For 32 antennas and 2 RF chains during the measurements, we used $N_{AM} = 2$ modules. At the conference, 4 modules were connected to the 64 antennas. A simplified block diagram of the modularization and the used hybrid architecture can be seen in Figure 1.

The RF chains of the testbed are realized with a National Instruments SDR NI USRP-2952R. This is a SDR similar to the popular Ettus USRP X310. It offers two RF chains with a

frequency range of 0.4GHz to 4.4GHz. Further information can be found in the datasheet [9]. The digital baseband signals are sent to respectively received from a host PC. It runs the digital signal processing of the hybrid analog-digital architecture. The signal processing will run off-line and is further described in Section IV. The host software also controls the phase and amplitude settings of the AMs and configures them according to the used algorithm.

The UE of the demonstration has $N_{UE} = 1$ antenna and we used one UE during the demonstration and measurement. The UE is implemented with our self-developed SDR ExsV. The ExsV offers four RF chains with a frequency range between 0.7GHz to 3.0GHz and a maximum bandwidth of 30MHz. The ExsV includes a field-programmable gate array (FPGA) for signal processing and control.

III. Analog Module Description

The analog module fully connects 2 to 16 ports in the RF domain. The network has one vector modulator per path. The network and the vector modulators are reciprocal and thus the AM can be used for time division duplex systems. Figure 3 shows the analog module and Table I summarizes the key parameters. The module offers a digital interface to control

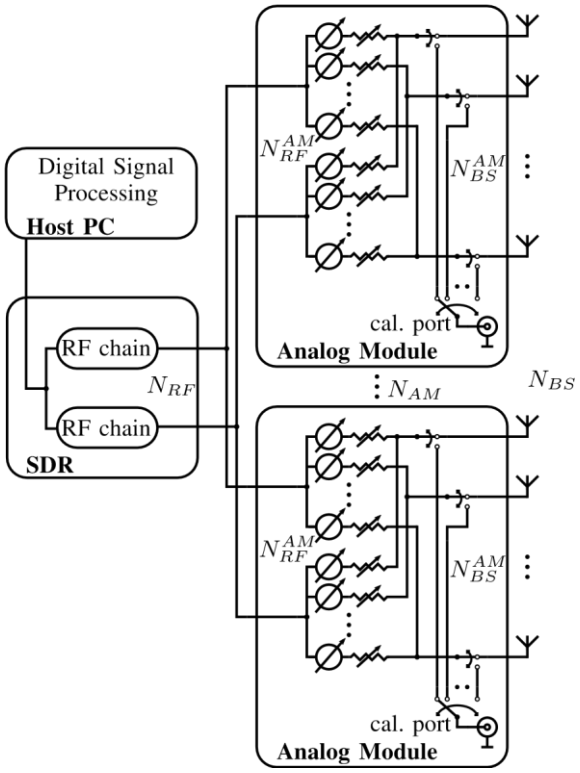

Fig. 1. Simplified system architecture of the BS for a Hybrid massive MIMO system

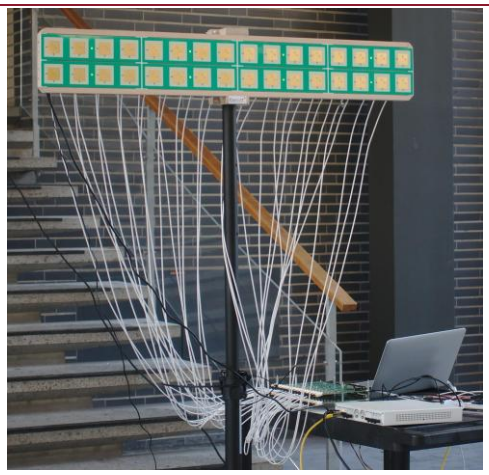

Fig. 2. The testbed during the measurements

the phase and amplitude of every vector modulator. A small FPGA in conjunction with digital-to-analog converters (DACs) converts this interface to analog control signals for the phase shifters and variable attenuators. Through the FPGA design, the interface can be adapted to the connected control instance, like the USRP SDR. The FPGA incorporates a memory and logic for storing and using calibration data.

The distribution respectively combination network is realized using Wilkinson power dividers. The phase shifter design is based on a typical varactor diode architecture. A 90°-hybrid coupler divides the input signal into two branches with a phase difference of 90°. The two branches are terminated with varactor diodes. The varactor diodes reflect the signals with a certain phase change. The phase change is dependent on a control voltage applied to the varactor diodes. The reflected signals are in phase combined by the 90°-hybrid coupler at the output. At the input, the reflected signals are 180° out of phase and canceled. The phase change between the input and output signal is equivalent to the phase change of the reflected signals by the varactor diodes. An inductor in series with each varactor diode increases the tunable phase range. One phase shifter has a tuning range between 190° and 210°. Therefore in the AM two of these phase shifters per path are used in series for a tuning range above 360°. The topology of the variable attenuator is very similar to the phase shifter. It uses PIN diodes and a 90°-hybrid coupler. Instead of the varactor diodes the PIN diodes change not the phase but the amplitudes of the reflected signals. This effect attenuates the output signal but does not reflect the signal back to the input. The power is absorbed by the PIN diodes. Between the vector modulator components and the output ports an additional calibration network respectively port was added. Through a switching matrix, the 32 paths can be connected to the calibration port. This enables to rerun the calibration of all vector modulators during the operation without the need to connect all 16 antenna ports to a calibration device.

The AMs used for the demonstration can operate in a frequency band 2.32GHz to 2.48GHz. Changing certain components of the AM can change the frequency band. This enables to manufacture modules for different frequency bands. Additional to the 2.4GHz version, we have planned and simulated a version for a frequency band between 3.4GHz and 3.8GHz. The bandwidth of the AM is depending on the tolerable phase and amplitude errors. The following error and resolution values are valid for a bandwidth of 20MHz.

The phase range of the AM is 360° and the attenuation range is 20dB. The limits by design of the phase and attenuation settings result in resolutions of more than 9bit each. The practical operation resolution is lower and restricted by the phase and amplitude errors. These errors occur not only within the settings range but also between the vector modulators of all paths. The module has to be initially calibrated to compensate for variations in component values, length differences, and other hardware imperfections. The calibration is carried out at a certain frequency. The errors increase as the difference between the signal frequency and the calibration frequency grows. Thus the calibration is necessary for multiple points within the frequency range of operation. Every calibration point is achieving the specified tolerances within the bandwidth of 20MHz. Figures 6(a) and (b) show the errors for one exemplary path at a frequency of 2.4GHz over the settings range. The maximum and RMS errors for all paths and all settings (with a resolution of 8bit) over the bandwidth can be seen in Figure 4. The RMS errors are smaller than the least significant bit for a 8bit resolution. This resolution is higher than offered by off-the-shelf variable phase shifters

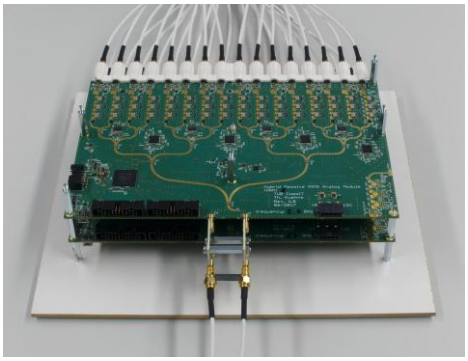

Fig. 3. A photo of two analog modules for 2 RF chains and 32 antennas

and attenuators especially taking into account that they are achieved over both the phase and amplitude settings range. It allows us to investigate and demonstrate the influence of the resolution in real-world scenarios. We expect to decrease especially the maximum error values with further work on the calibration setup. Since many beamforming algorithms only rely on phase modulation it is possible to calibrate the AM in a phase shifter mode. In this mode, the amplitude modulators are only used to compensate for the varying insertion loss of the phase modulators. The phase and amplitude errors for the phase shifter mode are smaller than for the full vector modulation mode. They are shown in Figure 5 and Figure 7.

The insertion loss of a calibrated AM measured between two ports is around 28dB. The exact value does vary with the calibration but is known after a calibration run. The insertion loss has two main parts, the power distribution network and the insertion loss of the components. The loss per path of the ideal power distribution network is 15dB. 12dB due to the 1 RF chain to 16 antennas network and 3dB due to the 2 RF chains per antenna network. Among others two of the reasons for the high additional insertion loss of 13dB are the physical size and the network size of the AM. The phase shifter and attenuator have a combined insertion loss between 5dB and 8dB depending on the phase setting. Furthermore, the connectors, calibration switches, imperfections of the power distribution, and the transmission lines (≈200mm per path) add also 5dB.

IV. Beam Alignment Demonstration

The testbed can be used to compare and investigate BA algorithms in a real propagation environment and with hardware imperfections. To demonstrate the capabilities of the testbed we implemented three algorithms for the BA problem and measured their performance. The three algorithms are an exhaustive search, a hierarchical bisection search based on [10] and an algorithm named Agile-Link [11]. The chosen algorithms have a low signal processing complexity. They can be used as a baseline comparison for future experimentation on more advanced algorithms like [12]. The results were measured at a carrier frequency of 2.4GHz in an indoor environment. The room was a large empty hall with a ground

TABLE I
Analog Module Parameters

Parameter	Value
RF chain ports	1
antenna ports	16
frequency range (2.4GHz version)	2.32GHz to 2.48GHz
bandwidth for error guaranties	20 M
phase range	360
typ. attenuation range	20dB
phase and attenuation resolution	8 b
phase RMS error	< 1.4
attenuation RMS error	< 0.12dB
phase resolution (phase shifter mode)	9 b
phase RMS error (phase shifter mode)	< 1.3
attenuation RMS error (phase shifter mode)	< 0.06dB
insertion loss (including 15dB power distribution)	28dB

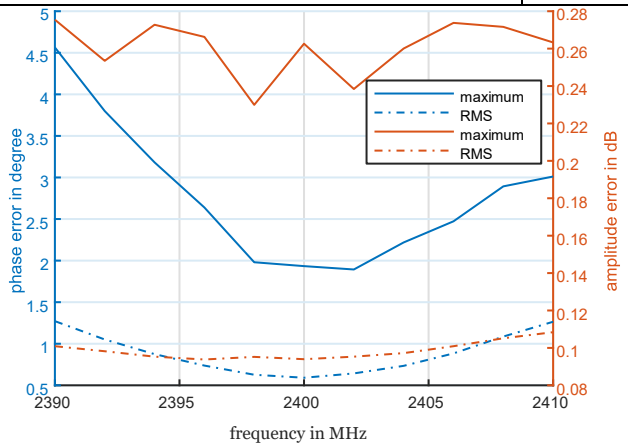

Fig. 4. Measured maximum and RMS phase and amplitude error over the bandwidth of the AM in the vector modulator mode with 8bit resolution calibrated at 2.4GHz

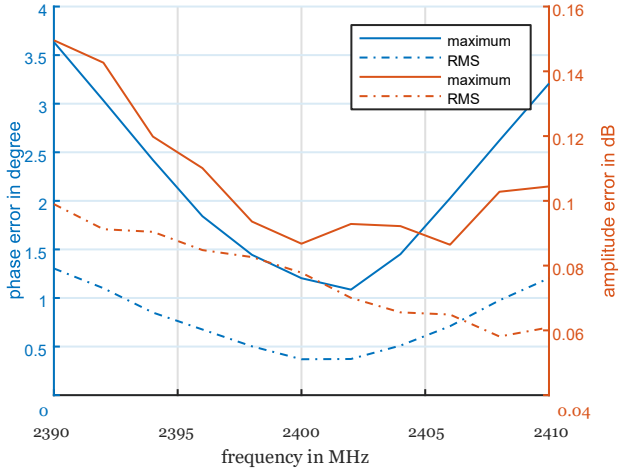

Fig. 5. Measured maximum and RMS phase and amplitude error over the bandwidth of the AM in the phase shifter mode with 9bit resolution calibrated at 2.4GHz

area 20m by 7m and a height of 6m. We only used beamforming at the BS with 32 antenna elements in a 2 by 16 configuration. The UE used a fixed beam antenna

with a gain around 6dB pointing towards the BS. The beam alignment tracked only AoAs from the front of the antenna array and in the azimuth within an angular interval $\phi \in [0°, 180°]$.

The elevation angle was not measured and we used a fixed elevation beam configuration during all measurements. Hence the goal of the BA algorithms was to find the AoA φ of the channel path with the highest gain.

The second and third of the measured algorithms were proposed to be used in millimeter-wave scenarios with the assumption of sparse channels, meaning a low number of multipath components. To evaluate these algorithms in such a scenario but at the carrier frequency of 2.4GHz we chose the specified room and antenna configuration. The room had a low number of reflectors creating sparse channels even in the sub-6GHz range. The directed antenna at the UE side pointing towards the BS created a strong line of sight (LOS) path. Additionally, both algorithms could also be extended to support multiple paths as described in the corresponding references. To check our assumptions of the channel we measured at all measurement locations a sweep of a narrow beam through the angular interval and compared it with the calculated values assuming only the LOS path. Figure 8 shows the comparison for the location of the results shown in section IV-B.

To measure the channel gain the UE transmitted periodically a training frame which was received by the BS. The training frame consisted of 4 Zadoff-Chu sequences each of length 32 in a bandwidth of 0.25MHz. The receiver signal processing detected the frame start and calculated the channel gain with a cross-correlation of the known sequence and the received samples. Since we only used beamforming on the BS side the BA algorithms could setup beam patterns and directly measure the associated channel gain. Although two RF chains for a hybrid beamforming processing were available we used them separately as two channels. No hybrid processing was strictly required by the selected algorithms.

A. Algorithms

The most basic solution for the initial acquisition is an exhaustive search. The AM and the antenna array is used as a

phased array with optimal phase coefficients [13, p. 1088] to form narrow beams with a certain beam direction respectively angle and a given beamwidth ψ. ψ is dependent on N_{BS} and the direction of the beam. The antenna directivity (ergo the array factor, ignoring the single element pattern) generated with the phased array is equivalent to the maximum possible directivity using a set number of elements. A codebook F of beamforming vectors is formed to cover the angular interval equidistant with $N = N_{BS} = 16$ beams. Figure 9(a) shows 3 of the 16 calculated beam patterns of the codebook. The exhaustive search algorithm checks every codeword of F and stores the corresponding channel gain. φ of the codeword with the highest channel gain is the resulting AoA. The exhaustive search requires N (in our case 16) training slots. For a simulation-based analysis of the exhaustive search algorithm see [14].

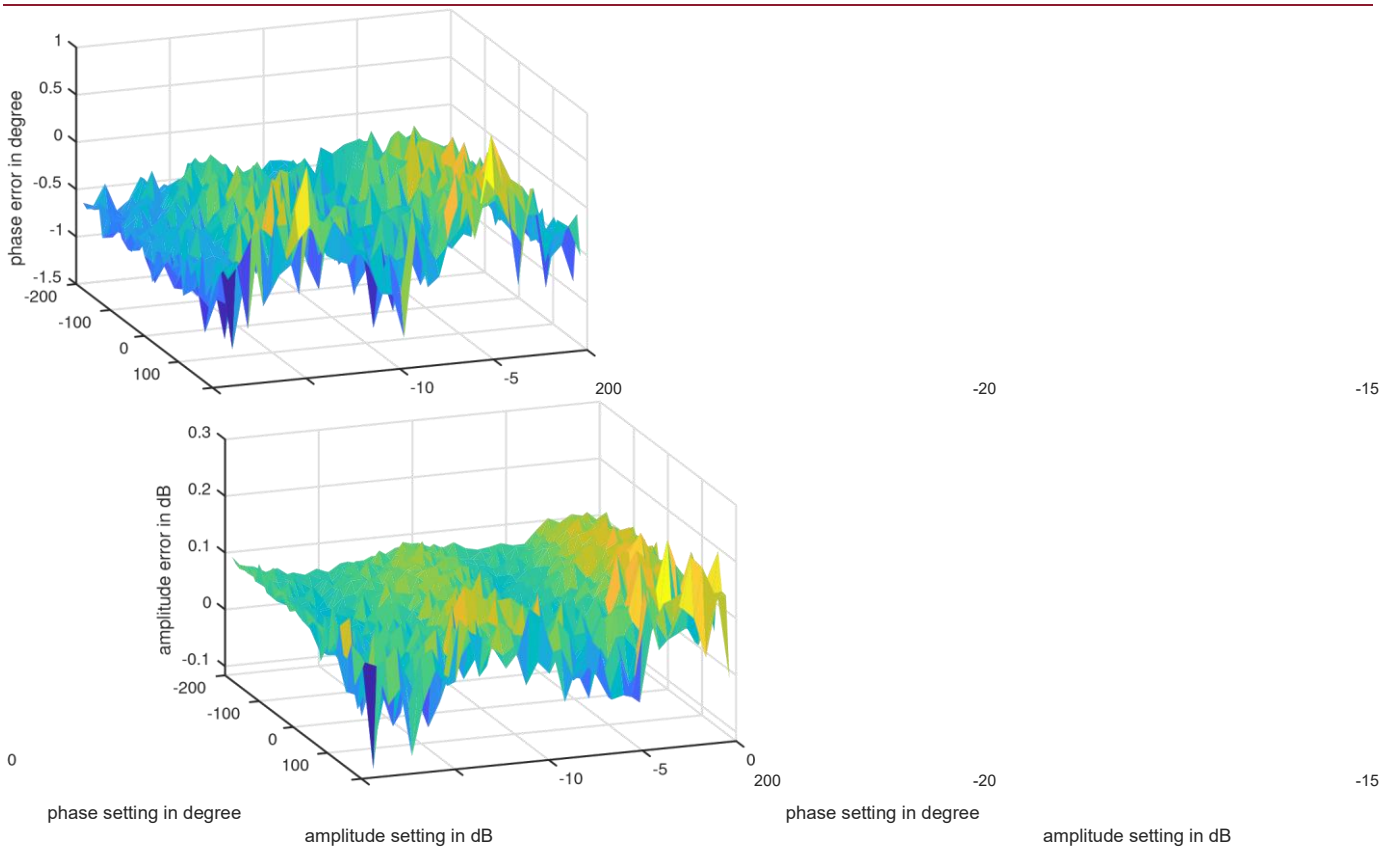

Fig. 6. Measured performance of one path of the AM in the vector modulator mode with 8bit resolution and calibrated and measured at 2.4GHz: (a) phase error over the settings range; (b) amplitude error over the settings range

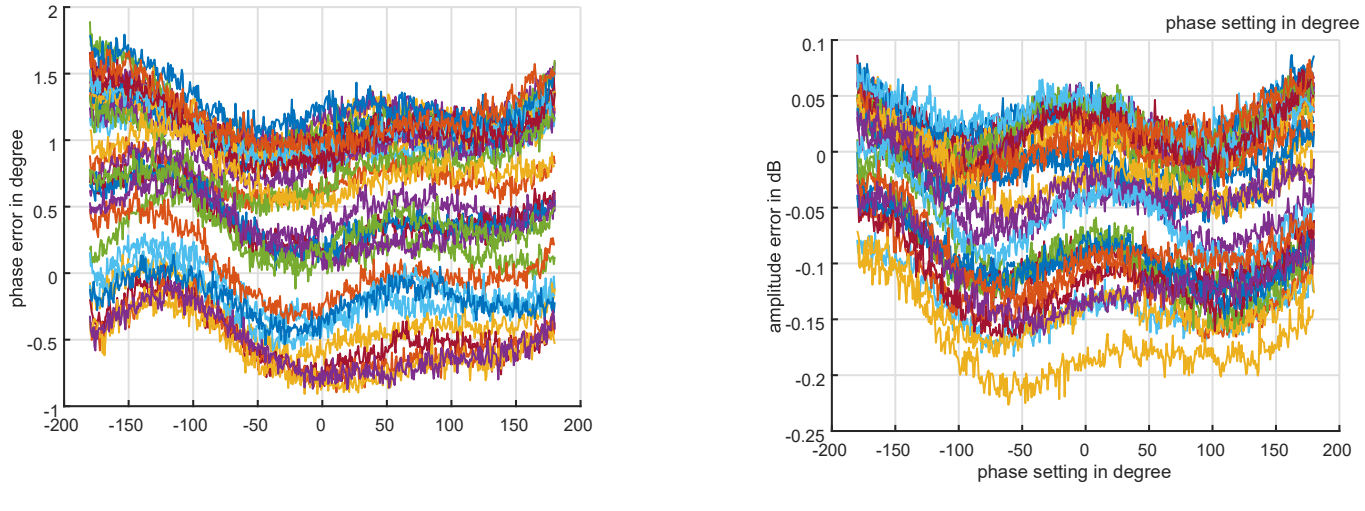

Fig. 7. Measured performance of all paths of the AM in the phase shifter mode with 9bit resolution and calibrated and measured at 2.4GHz: (a) phase error over the phase settings range; (b) amplitude error over the phase settings range

The second implemented algorithm is a hierarchical bisection search similar to the one described in [10]. The idea of a hierarchical bisection search is to use multiple codebooks in levels. F_s is a codebook of level $s = 1,2...S$ and S is the number of levels. A codebook of level s is divided into K^{s-1} subsets with K beamforming vectors in each subset k. One subset of a subsequent level is a refined version of a codeword of the previous level covering with K beams the angular interval covered by the one previous beam. A typical choice $K = 2$ means that the angular

interval of a beam is divided into 2 beams in the next level. $[F_{(s,k)}]_{:,m}$ is the beamforming vector m = 1,2..K in level s and subset k. The highest level has $N = N_{BS}$ = 16 beam vectors with the same angular resolution as the exhaustive search. The beamforming gain of codewords increases with the level of the codebook. Therefore a lower level has a higher probability of error finding the correct beam covering the AoA. This effect could be compensated but with cost applying a power allocation scheme for the different levels, for example, using multiple training frames in lower levels. To have a comparison of the basic versions of the algorithms we did not use any power allocation during the experiments. The search iterates through the levels of the codebook refining the beamforming. It uses the subset of beams corresponding to the beam with the highest channel gain found in the previous level. The implemented algorithm corresponds to Algorithm 1 of [10] but with only one UE antenna beam (respectively no loop over MS codewords in [10]). In contrast to [10] we did not use the proposed scheme for creating the beamforming vectors but a simpler algorithm. This is due to the low number of RF chains we could use to generate the necessary beam patterns. The proposed beamforming would perform very poorly with

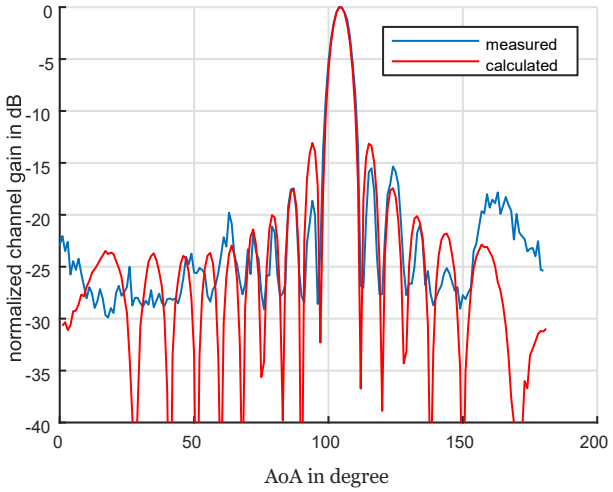

Fig. 8. Normalized measured and calculated (only LOS assumed) channel gain over the AoA with the 16 by 2 antenna configuration using a swept narrow beam.

only 2 RF chains. The possibility of the AM to modulate also the amplitude could circumvent this but with the cost of a lower beamforming gain. Therefore we generate the lower levels with a quadratic phase excitation as described in [15]. The flatness of the beams is worse than in [10] but is sufficient for our measurement. In other systems, this trade-off between simplicity respectively complexity and flatness of the beams would need additional investigation. The beams of the highest level are generated as in the exhaustive search. The calculated patterns are plotted in Figure 9(b). The codebook has S = 3 levels. The first two levels have K = 2 and the third level has K = 4. In this configuration, the hierarchical search needs 8 training slots to find the AoA. Additionally, we also measured with a S = 2 and K = 4 configuration. This is equivalent to skipping the first level of the first configuration resulting in the same number of necessary training slots. Though skipping the lowest level means skipping the level with the lowest beamforming gain and as a result improving the error probability over SNR.

The third algorithm is proposed in [11] and named Agile-Link. Contrary to the first two, it is not a search based algorithm. It does not scan the angular dimension with single beams but uses multiple beams randomly combined into one beamforming vector. The resolution is defined as angular interval over N with N possible AoAs. The algorithm combines (called hashing in the reference) the beams into B bins respectively hashes. Each hash is a combination of R sub-beams. [11] proposes to use sub-arrays, one for each subbeam, to generate patterns with beams in multiple directions. The phase excitation of the sub-arrays is calculated by the phased array method as used in the exhaustive search. Since a sub-array uses a reduced number of elements forming the sub-beam, each sub-beam has a R times wider beamwidth

and hence, $R = {}^{\mathrm{p}}N/B$. As also stated in [11] such a beam generation does create bad beams since the side-lobes and main-lobes of the sub-beams can sum up and deform the beam pattern. The authors propose to space the sub-beams in a large enough angular distance to minimize this effect. Agile-Link measures in one hashing step all bins and stores the corresponding channel gains. It repeats this step L times with random permutations of directions in the bins. AgileLink sets $L = \log N$ and $B = O(K)$ where K is the number of paths in the sparse channel. The random permutation does change the combination of directions of sub-beams within one bin respectively pattern. This step does randomly change the angular distance between the sub-beams. Therefore it can not be guaranteed that the interference between the main-lobes and the side-lobes of the sub-beams is minimized. It is unclear for us how the authors solved this problem for generating appropriate beam patterns. Since the AM is not restricted to phase modulation we used a different beam pattern generation. The calculation is similar to the phased array method which is equivalent to a Fourier transformation between the angular domain and the excitation coefficients of each

element [13, p. 1088]. In a phased array only one angular value (the beam direction) is non-zero resulting in an amplitude of 1 for all excitation coefficients. Multiple angular directions with non-zero values, as required with sub-beams forming one pattern, transform to a varying amplitude for different antenna elements. We change the phase and amplitude accordingly with the AM. Figure 9(c) shows one generated set of 4 bins. The drawback of this method is the decreasing directivity of around 12dB compared to a single beam direction. 6dB resulting from the generation of 4 directions in one pattern and 6dB due to the amplitude modulation (through attenuation). The codebook configuration for the measurement was $N = 16$, $B = 4$, $R = 4$ and $L = 4$. After $L \times B$ measurements a voting system chooses the AoA with the highest probability. Thus Agile-Link needs 16 training slots. The voting system is based on the idea, that the bin with the highest measured energy in one step gives votes to all directions which are hashed into that bin. To suppress the influence of side-lobes the actual beam patterns are used as a probability distribution for the directions included in the vote of the bin. The summation of the votes of the B bins results in a probability for each direction for the one hashing step. After L steps the product of probabilities gives the final estimation for the AoA. The highest probability is the AoA. Directions with lower but non-zero probability are multi-path components.

Table II lists the required training slots of the three algorithms. Agile-Link does not provide a reduction and the hierarchical search only by a factor of 2 in measurement time for the given setup. But both the hierarchical search and AgileLink scale in time better for a larger number of possible beam configurations than the exhaustive search. This is an important consideration for larger arrays and especially for BA between two stations with antenna arrays and beamforming. Please see [10] and [11] for the required number of training slots for arbitrary antenna elements.

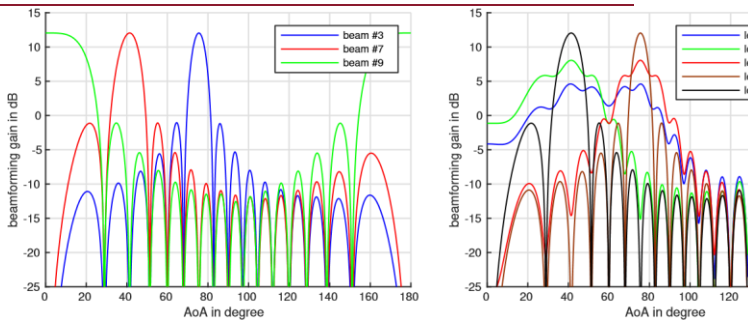

(a) (b)

Fig. 9. Exemplary calculated beam patterns for 16 horizontal elements for (a) e

TABLE II
COMPARISON OF THE REQUIRED TIME SLOTS FOR THE ESTIMATION (16 POSSIBLE AOAS)

Algorithm	Number of Training Slots
exhaustive search	16
hierarchical search $K = 2$ (one slot per level)	8
Agile-Link $L = 4$, $B = 4$	16

B. Results

The results shown in this section refer to one measurement location at an AoA of 115° with a distance of 11m between the BS and the UE. They are based on the same measurement run as Figure 8. The SNR is swept changing the transmission power of the UE in 3dB steps. Every SNR value was measured 200 times per algorithm and beamforming vector. Figure 10 shows the probability of error estimating the correct AoA. The exhaustive search shows the best performance. The 2 level hierarchical search algorithm has a gap of around 3dB and the 3 level configuration 5dB in comparison to the exhaustive search. The gap between Agile-Link and the exhaustive search is 11dB. Due to the limited number of SNR steps, the number of measurement iterations per point, and general precession of the SNR sweep a tolerance of ±1dB can be assumed. Taking this into account the size of the gaps is equal to the difference between the lowest beamforming gain of the codebooks and the gain of the exhaustive search patterns. The difference between the exhaustive search patterns and the lowest gain pattern of the 2 level hierarchical search at the AoA is 4dB, of the 3 level hierarchical search 7.4dB, and of Agile-Link 12dB.

The exact position and form of the error probability curves are not only influenced by the BA algorithms but also by the frame detection. If the frame could not be properly detected, the channel gain calculation is not correct. This can result in an estimation error for all three algorithms. Since the same frame detection mechanism is used for all algorithms the relation (the gap size) between

the error probability curves would not change with a different frame detection. The frame detection is necessary because the BS and UE are not time and frequency synchronous, as it would be in a Wi-Fi system. In a synchronous cellular system (for example with a separate control channel) no frame detection would be necessary. We run additional measurements without frame detection. The BS received a certain number of samples which guaranteed to record a complete continuous frame. The maximum received power within this period was used to calculate the channel gain. As can be seen in Figure 11 the absolute position of the error probability curves changed but the gaps stayed constant within the measurement accuracy.

Of cause, these observations do not take the number of required training slots into account. As already written in the algorithm description a power allocation scheme, for example, a simple average of training slots, could be used to enhance the error probability. Using the formulas for the number of required training slots, the power allocation scheme gain, and the difference in beamforming gain it is possible to compare the performance of the algorithms.

For Agile-Link a simple and adaptive way could be to increase L to improve the estimation error. However, this does not work for non-synchronous systems with frame detection. Agile-Link uses the product of L measurements of probabilities for a certain direction under the assumption that for the AoA direction always a correct but noisy channel gain is measured. This is not the case for a wrong frame detection due to a bad SNR.

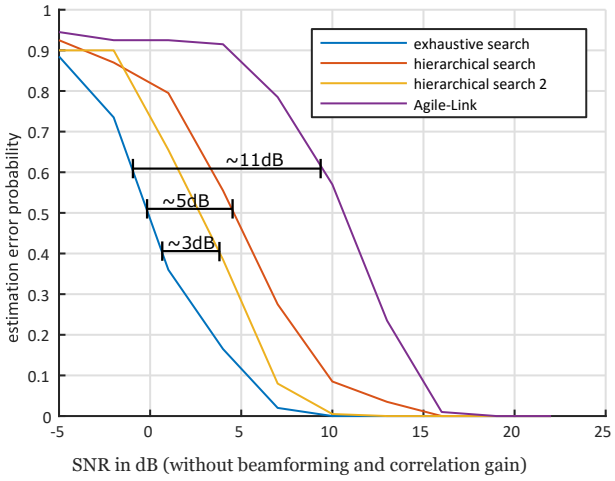

Fig. 10. Measured average probability of error estimating the AoA with frame detection.

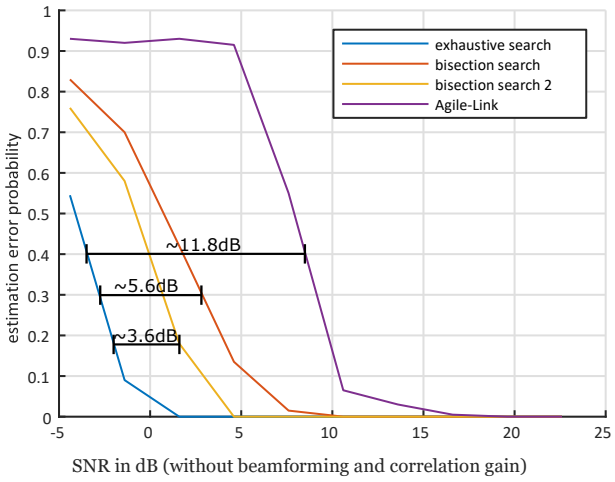

Fig. 11. Measured average probability of error estimating the AoA without frame detection.

V. Conclusion

In this paper, we have presented our hybrid massive MIMO testbed based on our self-developed AM. The testbed enables the investigation of signal processing for a hybrid analogdigital architecture. Multiple AMs can be interconnected to create different hybrid architectures and varying numbers of antenna elements or RF chains. The phase and amplitude resolution respectively error performance of the AM is more than sufficient for communication and fulfills experimentation and measurement requirements. We have demonstrated our testbed showcasing and measuring three basic BA algorithms. As an outcome of the measurements, we can conclude that for the three algorithms the difference in error probability over SNR is determined by the difference in antenna gain between the algorithms. With this relation and formulas for the number of required training slots a trade-off for designing a BA protocol and codebook can be found. In future work, we intend to compare and measure more sophisticated algorithms. In addition, we want to describe a formalism for arbitrary algorithms which shows the connection between antenna array gain, error probability and training time.

References

[1] M. Shafi, A. F. Molisch, P. J. Smith, T. Haustein, P. Zhu, P. D. Silva, F. Tufvesson, A. Benjebbour, and G. Wunder, “5g: A tutorial overview of standards, trials, challenges, deployment, and practice,” *IEEE Journal on Selected Areas in Communications*, vol. 35, no. 6, pp. 1201–1221, June 2017.

[2] T. S. Rappaport, S. Sun, R. Mayzus, H. Zhao, Y. Azar, K. Wang, G. N. Wong, J. K. Schulz, M. Samimi, and F. Gutierrez, “Millimeter

wave mobile communications for 5g cellular: It will work!" *IEEE Access*, vol. 1, pp. 335–349, 2013.

[3] A. F. Molisch, V. V. Ratnam, S. Han, Z. Li, S. L. H. Nguyen, L. Li, and K. Haneda, "Hybrid beamforming for massive mimo: A survey," *IEEE Communications Magazine*, vol. 55, no. 9, pp. 134–141, 2017.

[4] C. Shepard, H. Yu, and L. Zhong, "Argosv2: A flexible many-antenna research platform," in *Proceedings of the 19th Annual International Conference on Mobile Computing and Networking (MobiCom)*. New York, NY, USA: ACM, 2013, pp. 163–166.

[5] J. Vieira, S. Malkowsky, K. Nieman, Z. Miers, N. Kundargi, L. Liu, I. Wong, V. Owall, O. Edfors, and F. Tufvesson, "A flexible 100-antenna testbed for massive MIMO," in *Globecom Workshops (GC Wkshps), 2014*, Dec. 2014, pp. 287–293.

[6] T. Obara, T. Okuyama, Y. Aoki, S. Suyama, J. Lee, and Y. Okumura, "Indoor and outdoor experimental trials in 28-ghz band for 5g wireless communication systems," in *2015 IEEE 26th Annual International Symposium on Personal, Indoor, and Mobile Radio Communications (PIMRC)*, Aug 2015, pp. 846–850.

[7] National Instruments, "Ni wireless research handbook," 2016. [Online]. Available: http://www.ni.com/en-us/innovations/wireless/ software-defined-radio.html

[8] O. E. Ayach, S. Rajagopal, S. Abu-Surra, Z. Pi, and R. W. Heath, "Spatially sparse precoding in millimeter wave mimo systems," *IEEE Transactions on Wireless Communications*, vol. 13, no. 3, pp. 1499– 1513, March 2014.

[9] National Instruments, *SPECIFICATIONS USRP-2952*, Jul. 2017.
[Online]. Available: http://www.ni.com/pdf/manuals/374412d.pdf

[10] A. Alkhateeb, O. E. Ayach, G. Leus, and R. W. Heath, "Channel estimation and hybrid precoding for millimeter wave cellular systems," *IEEE Journal of Selected Topics in Signal Processing*, vol. 8, no. 5, pp. 831–846, Oct 2014.

[11] O. Abari, H. Hassanieh, M. Rodriguez, and D. Katabi, "Millimeter wave communications: From point-to-point links to agile network connections," in *Proceedings of the 15th ACM Workshop on Hot Topics in Networks (HotNets)*. New York, NY, USA: ACM, 2016, pp. 169–175.

[12] X. Song, S. Haghighatshoar, and G. Caire, "A scalable and statistically robust beam alignment technique for mm-wave systems," *CoRR*, vol. abs/1708.09433, 2017. [Online]. Available: http://arxiv.org/abs/1708. 09433

[13] S. J. Orfanidis, *Electromagnetic Waves and Antennas*. Rutgers University, 2004. [Online]. Available: http://www.ece.rutgers.edu/ ~orfanidi/ewa/

[14] S. Hur, T. Kim, D. J. Love, J. V. Krogmeier, T. A. Thomas, and A. Ghosh, "Millimeter wave beamforming for wireless backhaul and access in small cell networks," *IEEE Transactions on Communications*, vol. 61, no. 10, pp. 4391–4403, October 2013.